Journal of Engineering Science and Technology
Vol. 21, No. 2 (2026) 562 - 484

THE INFLUENCE OF DIFFERENT STIFFNESS ON VORTEX-INDUCED VIBRATION ENERGY GENERATION SYSTEM

FATIN ALIAS[1], MOHD AFIFI JUSOH[1], MOHD FAIZAL ALI AKHBAR[1], MOHD HAIRIL MOHD[1], ERWAN HAFIZI KASIMAN[3], MOHD ASAMUDIN A. RAHMAN[1,2,*]

[1]Maritime Technology & Naval Architecture Programme, Faculty of Ocean Engineering Technology, Universiti Malaysia Terengganu, 21030 Kuala Nerus, Terengganu, Malaysia
[2]Centre for Offshore Renewable Energy (CEFORE), Universiti Malaysia Terengganu, 21030 Kuala Nerus, Terengganu, Malaysia
[3]Faculty of Civil Engineering, Universiti Teknologi Malaysia, 81310 Skudai, Johor, Malaysia
*Corresponding Author: mohdasamudin@umt.edu.my

Abstract

The growing need for sustainable energy in the oil and gas industry has led to increased interest in renewable power sources. Vortex-Induced Vibration (VIV) energy harvesting offers a promising method for converting kinetic energy from fluid flow into electricity. The research focuses on qualifying the influence of structural stiffness on the performance of a single rigid circular cylinder in a VIV energy generation system. Numerical simulations were performed for a Single Degree of Freedom (SDOF) model using Computational Fluid Dynamics (CFD). The Reynold number of 37000 and stiffness values ranged from 60 N/m to 800 N/m were considered. Results indicate that an optimal stiffness of 600 N/m yields a peak power output of 6.10 W, demonstrating that structural stiffness is a critical factor in maximizing energy conversion efficiency. These findings offer valuable guidance for designing VIV energy generation system to capture energy from water flow more efficiently for clean and sustainable energy.

Keywords: CFD, Energy harvesting, Marine energy, Renewable energy, Stiffness, Vortex-Induced Vibration.

1. Introduction

Vortex-Induced Vibration (VIV) is a fluid-structure interaction phenomenon that occurs when a fluid flows past a bluff body, generating alternating oscillatory forces on the structure [1]. These forces can induce transverse vibrations, particularly when the vortex-shedding frequency approached or matches the natural frequency of the structure. In recent years, VIV has gained significant attention in the field of energy harvesting, where the periodic oscillations can be exploited to convert kinetic energy of fluid flow into usable electrical energy [2]. The potential for integrating VIV energy generation into marine renewable energy systems positions this mechanism as a promising and sustainable complement to conventional energy technologies [3, 4].

The fundamentals of VIV have been extensively studied, particularly in relation to the structural dynamics influenced by stiffness. Stiffness is a key parameter that determines the natural frequency of a structure [5]. When this frequency aligns with the vortex-shedding frequency, resonance occurs and leading to maximum energy transfer [6, 7]. Studies investigating variations in stiffness have demonstrated that this parameter significantly affects the oscillation amplitude and frequency, as well as the overall efficiency of energy harvesting [8]. For instance, a study explored the role of linear stiffness in VIV systems [9], where the authors found that increased stiffness helped stabilize oscillatory behaviour under high flow conditions by suppressing excessive vibration amplitudes, an essential factor for maintaining structural integrity. Similarly, subsequent works examined the effect of linear stiffness tuning on the lock-in phenomenon [10]. Their findings revealed that adjusting stiffness can synchronize the structure's natural frequency with the vortex-shedding frequency, thereby significantly enhancing energy conversion efficiency [11].

Experimental studies on dual-beam configurations with linear stiffness have shown that specific stiffness values can maximize vibration amplitude and broaden the operational bandwidth for energy harvesting [12]. These finding highlight the importance of optimizing structural parameters in the design of VIV harvesters. Similarly, a novel self-tuning VIV energy harvesting system demonstrated that dynamically varying the linear stiffness during operation significantly enhance energy capture across a range of flow velocities, highlighting the effectiveness of stiffness modulation for adaptive performance [13]. More recent advancements further confirm that linear stiffness plays a pivotal role in achieving sustained resonance conditions while improving both stability and energy conversion efficiency in VIV systems [14].

Despite these advances, most prior investigations have focused on low-to-moderate Reynolds number (Re) regimes, where laminar or transitional flows dominate. In contrast, high Reynolds number conditions ($Re > 10^4$), which are characteristic of real-world marine currents introduce more complex flow dynamics, including turbulent wake interactions and vortex disorganization, that can significantly influence VIV performance. Although some recent studies have explored stiffness modulation and nonlinear restoring forces in turbulent flows [15], the combined influence of stiffness variation and high Re on energy harvesting performance remains insufficiently explored, particularly under fully turbulent regimes.

To address this gap, the present study investigates the impact of structural stiffness on the performance and efficiency of VIV energy harvesting under high Reynolds numbers of conditions using a Computational Fluid Dynamics (CFD) approach. Simulations are conducted using Altair HyperWork software, employing a fluid-structure interaction (FSI) model with a dynamic mesh.

This study investigates a single circular cylinder with variable linear stiffness values subjected to a range of flow velocities corresponding to a Reynolds number of 37,000, a regime dominated by unsteady vortex shedding. To accurately capture the complex vortex dynamics in the cylinder wake, the SST k − ω turbulence model is used. This model combines the strengths of the SST k − ω formulation near the wall in the free-stream, improving predictions of flow separation and vortex shedding as key factors in VIV [16]. The Reynolds-Averaged Navier-Stokes (RANS) equations are solved to efficiently describe the overall flow behaviour while maintaining computational feasibility at this high Reynolds number.

The study focuses on evaluating the effects of varying structural stiffness on VIV characteristics. Key output parameters include oscillation amplitude, frequency and energy conversion efficiency. The main objective is to evaluate how variations in structural stiffness influence VIV characteristics under high-Re conditions and to identify ideal stiffness values that maximize energy extraction efficiency without compromising structural stability. The findings aim to bridge the existing knowledge gap and provide practical design guidance for developing robust VIV energy harvesting systems suitable for realistic, turbulent marine environments. This research highlights the critical role of stiffness that contribute in order to enhance energy generation. The findings of this study will offer valuable guidance for development of next-generation hydrodynamic energy harvesting systems.

Novel contributions and objectives of the study

Stiffness is a fundamental structural parameter that governs the amplitude response and efficiency of vortex-induced vibration (VIV) energy generation system. Both experimental and numerical studies have demonstrated that stiffness directly influences the oscillatory behaviour of the cylinder and also controlling the balance between vibration growth and overall system stability. In general, higher stiffness suppresses oscillation amplitude.

Early numerical by Wan and Patnaik [17] reported through simulations that increasing intermediate stiffness values significantly reduced vibration response. In addition, Zahari et al. [18] experimentally confirmed that even across a range of stiffness conditions the maximum amplitude reached only 0.0065 m, highlighting the restrictive role of stiffness. Similarly, Sanaati and Kato [19] and Martins and Avila [20] observed that increasing stiffness or structural tension consistently limited vibration amplitude and reduced energy harvesting potential. By contrast, lowering stiffness encourages stronger oscillations and greater efficiency, though only within dynamically stable operational ranges. Zhang et al. [21] experimentally demonstrated that reduced stiffness conditions led to large oscillations, achieving efficiencies as high as 40.44%.

Likewise, Paré-Lambert and Olivier [22] numerically varied dimensionless stiffness and showed that oscillation amplitude is strongly stiffness-dependent, peaking at an efficiency of 10.6% under optimal stiffness values. Arionfard and Nishi [23] further supported these finding by testing three spring stiffness cases and

showing that both amplitude and efficiency (up to 31.4%) were significantly influenced by stiffness and the length ratio of the system. Overall, the findings clearly show that stiffness is a key factor in VIV performance. When the stiffness structure is high, oscillations are greatly reduced, limiting its ability to harvest energy. In contrast, lower stiffness allows larger vibrations and improves energy-harvesting efficiency, while still keeping the system dynamically stable.

Some studies emphasized the existence of optimal stiffness values that maximize energy harvesting performance. Barrero-Gil et al. [24] demonstrated experimentally and analytically that an optimal combination of mass, damping, and stiffness parameters produces peak amplitude ratios and maximizes efficiency. Similarly, Sun et al. [25] observed that although increasing stiffness generally reduces oscillation amplitude, local efficiency optima still arise at intermediate stiffness values, indicating that partial flexibility is necessary for effective energy harvesting. Dahl et al. [26] further confirmed that frequency ratios, which effectively modify stiffness characteristics, significantly influence amplitude shifts and synchronization behaviour.

Expanding on these findings, Ding et al. [27] numerically investigated asymmetric stiffness and showed that coupled oscillations altered the vibration response, while Gonçalves et al. [28] explored stiffness ratios in the range of 0.3–3.0 and found that oscillation amplitudes varied systematically with the ratio, with higher ratios enhancing vibration levels. In Gonçalves et al. [29] also highlighted the effect of fixed stiffness in two-degree-of-freedom systems, reporting that vibration decreased at smaller L/D ratios. In addition, Zhao et al. [30] showed that spacing variations, which indirectly modify effective stiffness, yielded a maximum amplitude ratio of A/D = 0.7 when L = 1.5.

In contrast, Zhao and Cheng [31] offered an alternative perspective by demonstrating numerically that maximum amplitude can also occur at high effective stiffness, suggesting that the relationship between stiffness and performance depends strongly on Reynolds number, structural constraints, and the prevailing flow regime. More recently, Gao et al. [32] reinforced these insights by showing that even fixed linear stiffness values continue to shape oscillatory amplitude in numerical modelling. Collectively, these studies highlight that stiffness cannot simply be classified as “low” or “high”. Instead, it must be carefully tuned often at intermediate or system-specific values in order to balance structural stability with amplitude growth and achieve optimal energy harvesting efficiency.

Although these studies provide important insights, several limitations remain. Most prior investigations were conducted at low-to-moderate Reynolds numbers, where laminar or transitional flow dominates. However, high Reynolds number flows introduce turbulent wake interactions that significantly affect vortex shedding coherence and vibration response. While a few recent studies have examined stiffness under turbulent conditions, a systematic stiffness sweep under fully turbulent, high Reynold number conditions for energy harvesting applications is still lacking. Previous work rarely evaluates wide stiffness ranges or identifies optimal stiffness that maximize power output in realistic marine environments. To clarify this gap, a comparative summary of existing research is presented in Table 1.

Table 1. Comparison of previous review papers and novelties of this review paper.

Authors	Method	Reynolds Number	Stiffness	Amplitude Ratio	Limitation
Wan and Patnaik [17]	Numerical Simulation	-	Intermediate stiffness	Reduced at higher stiffness	Moderate Re; no energy harvesting analysis
Zahari et al. [18]	Experimental	-	Range of stiffness values tested (not specified)	Max amplitude = 0.0065 m	No power evaluation: stiffness range limited
Zhang et al. [21]	Experimental	-	Constant stiffness (tested)	Significant oscillation for low stiffness	Only low stiffness tested; no high-Re analysis
Paré-Lambert and Olivier [22]	Numerical Simulation	200	Dimensionless stiffness varied	Max amplitude related to stiffness, varies	Re = 200; laminar regime
Ding et al. [27]	Numerical Simulation	100	Asymmetric stiffness varied	Coupled oscillations impact amplitude	Re = 100; laminar
Gambarine et al. [33]	Experimental	0.2×10^4 to 2×10^4	Stiffness ratio kx/ky = 0.3 – 3.0	Varies by stiffness ratio	No harvesting focus
Sun et al. [25]	Experimental	30,000 – 120,000	Stiffness varied by system	Higher stiffness reduces amplitude	System-specific; no systematic stiffness sweep
Sanaati and Kato [19]	Experimental	1,000 – 16,000	Four tension values (impact stiffness)	Higher tension = reduced amplitude	-Re limited (1000–16000); no harvesting study
Arionfard and Nishi [23]	Experimental	2,880 – 22,300	Three spring stiffness values	Amplitude depends on stiffness & L*	Limited stiffness cases; Re < 22,300
Zhao and Cheng [31]	Numerical Simulation	300	Not varied	Amplitude comparable for L/D = 1 and 2	-
Barrero-Gil et al. [24]	Experimental & Analytical	High Reynolds	Mass-damping varied (affects stiffness)	Peak A/D for optimal mass-damping	No explicit CFD modelling
Wu et al. [34]	Review	Not applicable	General stiffness observations	Multi-mode vibration	No harvesting assessment

Table 1 (continue). Comparison of previous review papers and novelties of this review paper.

Authors	Method	Reynolds Number	Stiffness	Amplitude Ratio	Limitation
Chen et al. [35]	Numerical Simulation	55 – 200	Effective stiffness varied	Max amplitude at high stiffness	Re < 200; laminar
Zhao et al. [30]	Numerical Simulation	150	Spacing ratio L varied (stiffness impact)	Max A/D = 0.7 at L = 1.5	Re = 300; limited turbulence
Dahl et al. [26]	Experimental	11,000 – 60,000	Frequency ratios impact stiffness	Amplitude shifts with frequency ratio	No power calculation
Gonçalves et al. [29]	Experimental	2,800	Fixed stiffness for small L/D	Amplitude decreases with lower L/D	Not targeted at harvesting
Martins and Avila [20]	Numerical Simulation	1.5×10^3 – 3.5×10^4	Damping & stiffness varied	Higher stiffness reduces amplitude	Not targeted at energy harvesting
Gao et al. [32]	Numerical Simulation	-	Fixed linear stiffness	Amplitude affected by fixed stiffness	No stiffness variation
Gonçalves et al. [28]	Experimental	2,800	Fixed stiffness	Vibration affected by fixed stiffness	Limited geometric variation
Barrero-Gil et al. [24]	Experimental & Analytical	High Reynolds	Constant stiffness	Optimal stiffness improves vibration	Max efficiency achieved

Although many studies have explored stiffness effects in VIV systems, most investigations were performed under laminar or transitional flow regimes, involved limited stiffness ranges and also did not quantify energy harvesting performance. To date, no study has systematically evaluated a broad stiffness range (60–800 N/m) under fully turbulent, high Reynolds number flow (Re = 37,000) to determine the design of stiffness for maximizing energy generation from VIV.

This study addresses these gaps by employing a fully using CFD approach, with dynamic mesh motion and the SST k–ω turbulence model to accurately resolve wake dynamics. The work provides new insights into how stiffness influences vibration amplitude and power output in hydrodynamic flow conditions.

The objectives of this study are:

- To numerically evaluate the influence of a wide range of stiffness values on VIV response under high Reynold number turbulent flow.
- To quantify how stiffness affects oscillation amplitude and energy conversion using a fully CFD model.

- To determine the ideal stiffness value that maximizes energy output by evaluating through calculations while ensuring structural stability.

2. Materials and Methods

2.1. Geometrical modelling and boundary condition

In a fluid channel, simulations were conducted on the flow of an unsteady, Newtonian, and incompressible fluid past a cylinder. The equations that govern fluid motion are referred to as the Navier-Stokes equations.

2.1.1. Continuity equations

The continuity equation, often referred to as the instantaneous mass conservation equation, is formulated by applying the principle of mass conservation to a control volume in the case of a general fluid, as shown in Eq. (1) [36].

$$\frac{\partial \rho}{\partial t} + \nabla . (\rho \, \vec{u}) = 0 \tag{1}$$

where ρ is the fluid density, t is time, $\vec{u}$ is the flow velocity vector.

The first term $\frac{\partial \rho}{\partial t}$ denotes the rate of change of density with respect to time. Meanwhile, the second term $\nabla . (\rho \, \vec{u})$ expresses the divergence of the vector field $\rho \, \vec{u}$ at a specific point fixed in space. Eq. (2) provides an expression for the continuity equation that can also be represented through the use of the substantial derivative [36]:

$$\frac{D\rho}{Dt} + \nabla . (\rho \, \vec{u}) = 0 \tag{2}$$

2.1.2. Momentum equations

The conservation equation for momentum is derived by applying Newton's second law of motion to the fluid control volume, where the rate of change of momentum of a fluid particle equals the sum of surface and body forces acting on it. This is valid for any continuum fluid, including liquids and gases. The momentum equation is expressed in Eq. (3) [37]:

$$\rho \frac{\partial \vec{u}}{\partial t} + \, (\rho \, \vec{u} \, \cdot \, \nabla) = 0 - \nabla \mathrm{p} + \rho \mathrm{b} + \nabla \cdot \tau \tag{3}$$

where p is the pressure, b is the source term (generally gravity), τ is the viscous stress tensor.

For Newtonian fluid, the viscous stresses are directly proportional to the rate of strain. Under this assumption, the stress tensor in Eq. (4) can be simplified using the Stokes hypothesis when applied to a Newtonian fluid [37]:

$$\tau_{ij} = \mu(\frac{\partial u_i}{\partial x_j} + \frac{\partial u_j}{\partial u_i}) - \frac{2}{3}\mu\delta_{ij}\frac{\partial u_k}{\partial u_k} \tag{4}$$

where μ is the dynamic viscosity of the fluid.

Following the completion of several validation procedures, the turbulence model of k-ω was selected for use in the simulation in the CFD study. This choice was made based on the flow characteristics and the level of accuracy required for

modelling turbulent behaviour, particularly in resolving the background velocity profile and wake dynamics.

In this research, the simulation is based on a Single Degree of Freedom (SDOF) system, as illustrated in Fig. 1, where a rigid circular cylinder is attached to a linear spring (with stiffness, k) and a damper (with damping coefficient, c). The choice of an SDOF framework is intentional, allowing the study to isolate and analyse the influence of structural stiffness on transverse vortex-induced vibrations and the resulting energy harvesting performance. By restricting the motion to the transverse direction, the model reduces complexity inherent in multi-degree-of-freedom systems while still capturing the dominant dynamics of interest [38]. This simplification enables a clear interpretation of the primary energy conversion mechanism, which is governed by vortex shedding and lock-in behaviour. It also provides a computationally efficient framework for evaluating the effect of varying stiffness parameters under turbulent flow conditions.

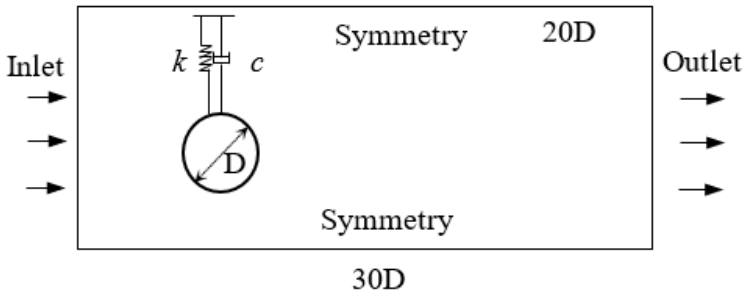

Fig. 1. Schematic drawing of a cylinders (not to scale).

Although real-world VIV systems often exhibit coupled transverse and inline (2DOF) motions, numerous studies have shown that transverse vibrations dominate energy harvesting potential due to their larger amplitude and stronger fluid-structure interactions [39]. Moreover, SDOF models have been extensively validated in the literature and are widely recognized as a foundational tool in VIV research, capable of capturing the essential physics while maintaining computational efficiency [40].

The SST k-ω model introduces two additional transport equations: one for the turbulent kinetic energy k (Eq. 5) and one for the specific dissipation rate ω (Eq. 6). These governing equations, which define the evolution of turbulent kinetic energy and its Turbulent Kinetic Energy (k), Specific Dissipation Rate (ω) are expressed as follows:

$$\frac{\partial k}{\partial t} + U \cdot \nabla k = \nabla . [\left(v + \frac{v_t}{\sigma_k}\right)(\nabla k)] + P_k - \beta^* k\omega \tag{5}$$

$$\frac{\partial k}{\partial t} + U \cdot \nabla_\omega = \nabla . [\left(v + \frac{v_t}{\sigma_\omega}\right)(\nabla_\omega) + \alpha \frac{\omega}{k} P_k - \beta\omega^2 \tag{6}$$

where $P_k = v_t(\nabla U : \nabla U)$ is the production term of turbulent kinetic energy, $v_t = \frac{k}{\omega}$ is the eddy viscosity, $\sigma_k, \sigma_\omega, \alpha, \beta \; and \; \beta^*$ are model constants.

In the present CFD work, the k-ω turbulence model was used for the simulations following several validation steps, selected based on the flow characteristics and the

level of accuracy required for modelling turbulent behaviour, particularly in representing the background velocity profile and wake dynamics.

Table 2 presents the physical parameter values used in the present model. The inlet flow velocity was set to achieve a Reynolds number of 37000. For the cylinder configuration, parameters such as Reynolds number, damping ratio and mass ratio were kept constant, while the spring stiffness was systematically varied across a specified range to examine its effect on VIV response. Both spring stiffness and reduced velocity are known to significantly influence the VIV behaviour, as they directly affect the resonance conditions and the resulting oscillation amplitude.

Table 2. Physical parameter for present model.

Parameter	Value
Mass ratio (m*)	2.36
Diameter ratio, d/D (m)	0.0554
Damping ratio (ξ_{total})	0.006
Reduced Velocity (V_r)	2-14
Reynolds Number (Re)	37000
Density ρ (kg/m^3)	1025
Kinematic viscosity υ	1.1×10^{-3}
Spring stiffness K (N/m)	60 - 800

To quantify the energy transferred from the fluid flow to the oscillating cylinder, the total energy and power generated during one oscillation cycle, *Eviv* are calculated using Eq. (7) and Eq. (8):

$$E_{VIV} = \frac{1}{2}KA^2 + 2\pi^2 C_{total} f_{osc} A^2 \tag{7}$$

$$P_{VIV} = \frac{1}{T_{osc}} E_{VIV} \tag{8}$$

where K is the spring stiffness, A is the amplitude of the waves, C_{total} is coefficient of damping in a system, f_{osc} is the cylinder's vibration frequency and the flow of VIV power is evaluated throughout an oscillation cycle [41].

In these equations, K represents spring stiffness, A is the vibration amplitude, C_{total} is the total damping coefficient and f_{osc} refers to the oscillation frequency of the cylinder. The flow of VIV power is evaluated over one complete oscillation cycle, allowing for accurate characterization of the harvested energy [41]. The power-to-volume density, P_{VIV_V}, was then computed using the power generated by cylinder. as expressed in Eq. (9):

$$P_{VIV\_V} = \frac{P_{VIV}}{Volume} \tag{9}$$

The boundary conditions applied to the computational domain are summarized in Table 3. A pressure outlet was assigned at the downstream boundary to allow for the smooth exit of flow, while slip wall conditions were implemented on the lateral boundaries to eliminate shear stress simulate far-field behaviour. Viscous stresses were also neglected at the outlet to prevent artificially influences on the wake dynamics. It is important to note that positioning the outlet boundary too close to the cylinder or wake region can lead to non-physical pressure wave reflections, potentially compromising the accuracy of both the flow field and the structural

response. Hence, careful attention was given to the size and placement of domain boundaries in order to ensure realistic and stable simulation outcomes.

To mitigate the risk of non-physical pressure reflections and ensure accurate flow development, the downstream length of the computational domain was extended sufficiently to allow vortices and flow disturbances to dissipate naturally before reaching the outlet. In this study, the outlet boundary was placed 20D downstream (20 times the cylinder diameter) from the cylinder centrelines. This domain length was selected based on recommendations from existing literature and further validated through sensitivity testing to ensure that no backflow or artificial reflections influenced the flow field or structural response. A time step of 0.05 s was used to numerical stability throughout the simulation.

Table 3. The boundary Condition of the Present Model.

Type of boundary conditions	Surface Name
Wall	Cylinder
Symmetry	Top, Bottom and Sides
Inflow	Inlet
Outflow	Outlet

2.2. Mesh independence study

A mesh independence study was conducted to verify the numerical accuracy and stability of the simulation results. Given the high Reynolds number regime, particular attention was devoted to the near-wall mesh resolution to ensure accurate turbulence modelling. To resolve the boundary layer flow accurately, a wall-resolved approach was adopted by maintaining the non-dimensional wall distance (y^+) below 1 in the first cell adjacent to the cylinder surface.

This approach eliminates the need for wall function approximations and ensures precise capturing of the viscous sublayer dynamics and wall shear stresses. Local mesh refinement was applied around the cylinder region to adequately resolve vortex shedding and fluid–structure interaction effects. The mesh was iteratively refined until key output parameters, such as lift and drag coefficients, vibration amplitude and power output are converged within acceptable tolerances, confirming mesh independence.

Figure 2 illustrates the computational domain and the mesh layout surrounding the cylinder, including a close-up view of the refined mesh near the cylinder surface where steep velocity and pressure gradients are anticipated. The domain was discretized using unstructured triangular elements, allowing for greater flexibility in capturing complex geometries and flow features. Mesh refinement was strategically applied particularly in the wake region and near the cylinder to accurately capture the flow separation and vortex shedding.

A mesh convergence study was conducted by testing several mesh resolutions ranging from approximately 80,000 to 300,000 elements. The normalized transverse amplitude (Ay/DA), was used as the primary indicator of mesh sensitivity, representing the time-averaged vibration response of the cylinder. As shown in Fig. 3, the variation in Ay/D values became negligible converging to approximately 0.23 when the total element count was between 110,000 and 250,000. This indicates that the results became independent of the mesh resolution

within this range, thereby validating the adequacy of the chosen mesh for all subsequent simulations.

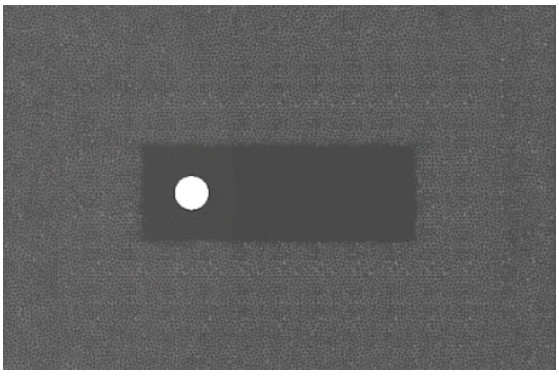

(a)

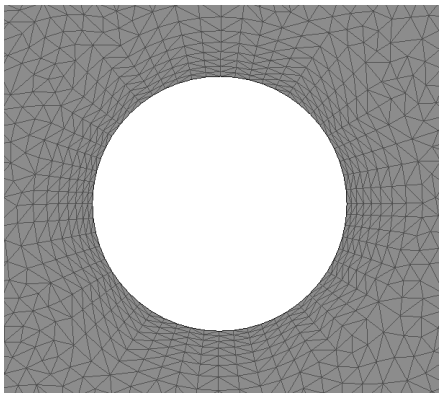

(b)

Fig. 2. Computational domain meshes of a cylinder. (b) Illustration of close-up mesh.

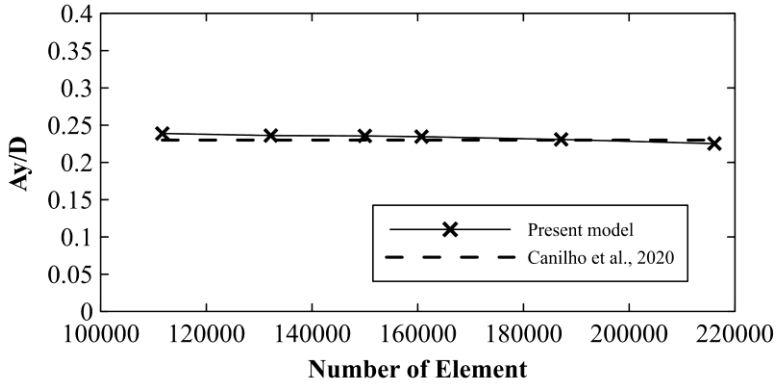

Fig. 3. Mesh independence study for present model.

2.3. Model validation

Validation was conducted in order to confirm the accuracy and effectiveness of the computational approach utilized in the current CFD model. The validation of current model was based on the study by Canilho et al. [42]. The graph in Fig. 4 demonstrates a strong agreement between the simulation results and the reference data, thereby supporting the validity of the model. Additionally, the result highlights that a significant reduction in the oscillation amplitude with increasing flow velocity in the lower velocity range, as predicted by the numerical simulations.

The graph presents a comparison of the dimensionless transverse amplitude Ay/D as a function of the reduced velocity Vr. The simulation results from the present study show good agreement with the published literature, validating the model's predictive capability. The model accurately captures the characteristic VIV response, including the sharp rise in amplitude within the lock-in region, with a peak occurring near $Vr \approx 7$, followed by a gradual decay beyond this region.

This behavior is consistent with the theoretical framework of VIV, which predicts that resonance occurs when the vortex shedding frequency synchronizes with the natural frequency of the structure, resulting in a significant amplification of motion [43]. The present model successfully captures this phenomenon and effectively simulates the post-lock-in regime where the amplitude declines as reduced velocity increases, indicating a reduction in fluid-structure coupling as synchronization ceases. These features confirm that the current CFD approach not only aligns with established experimental findings but also reproduces the theoretical dynamics of VIV dynamics, thereby validating the model's reliability and predictive accuracy.

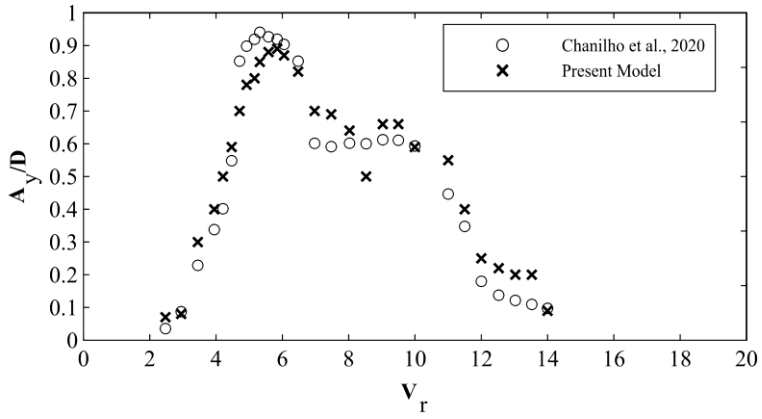

Fig. 4. Comparison and validation of the amplitude frequency between present model and Chanilho et al. [42].

A cylinder is said to be "locked-in" when the frequency of oscillation is equal to the frequency of vortex shedding. In this region, the largest amplitude oscillations occur. To further strengthen the validation, the frequency of oscillation was compared with the published results, as shown in Fig. 5. The predicted frequency variation agrees closely with experimental observations across the full range of reduced velocities. The variation of the normalized vibration frequency

ratio with reduced velocity for both linear and nonlinear stiffness systems. At low reduced velocities, both the vibration frequency F_V and vortex shedding frequency F_{VS} were unsynchronized, indicating that vortex shedding was not yet fully developed due to the weak fluid–structure coupling. As the flow velocity increased, the frequencies gradually aligned, initiating the lock-in regime.

More importantly, the model successfully replicates the evolution of the frequency ratio, a key indicator of synchronization during lock-in. The frequency ratio approaches unity within the lock-in regime, confirming that the numerical simulation accurately resolves the vortex shedding structure interaction. Beyond lock-in, the ratio progressively deviates from 1.0, matching the behaviour reported in the literature and reflecting the transition back to non-synchronized flow.

The combined agreement in amplitude, oscillation frequency and frequency ratio demonstrates that the current CFD approach reliably reproduces both the qualitative and quantitative dynamics of VIV. These results confirm that the model aligns with established published literature, thereby validating its predictive capability for subsequent parametric analysis.

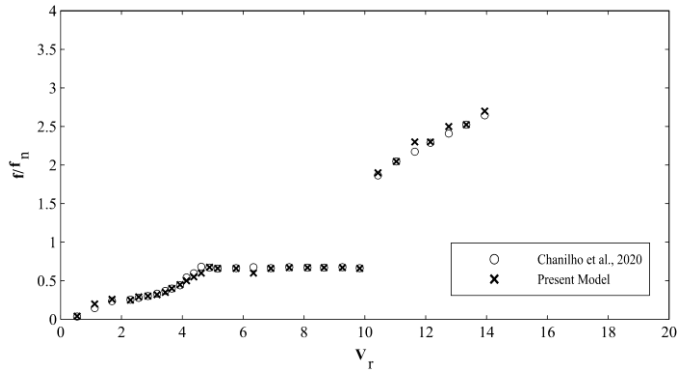

Fig. 5. Comparison and validation of the frequency of oscillation between present model and Chanilho et al. [42].

3. Result and Discussion

The results presented in Fig. 6 reveal a clear relationship between spring stiffness and the dimensionless maximum vibration amplitude in a VIV energy generation system. This trend carries significant implications for system design and performance optimization. At low stiffness values which are ranging from 66.67 N/m to 160 N/m, the vibration amplitude decreases steadily from 0.23895 to 0.21625, corresponding to a reduction of approximately 9.5%. This decline indicates that lower stiffness allows for high structural vibration, likely due to stronger resonance effects when the natural frequency of the structure closely aligns with the vortex shedding frequency [18].

In the mid-range stiffness values between 200 N/m to 500 N/m, the vibration amplitude experiences a sharper decline, decreasing from amplitude of 0.20605 to 0.18535, which represents a reduction of approximately 10.1%. This range marks a critical transition zone, where increasing stiffness begins to significantly suppress the ability of energy generation system to resonate effectively with the vortex

shedding frequency. As stiffness continues to rise beyond optimal levels, the structural response weakens due to a loss of synchronization between the vortex shedding and the natural frequency of the structure [44]. The data also indicate diminishing returns in vibration amplitude, demonstrating that excessive stiffness can negatively affect the efficiency of VIV energy generation systems.

At high stiffness values ranging from 600 N/m to 700 N/m, the vibration amplitude drops significantly, from 0.17995 to 0.00745. This rapid decline highlights the inability of overly stiff systems to effectively extract energy from the flow, as they fail to synchronize with vortex shedding frequency. The significant reduction in oscillatory amplitude indicated that excessive stiffness imposes strong mechanical constraints that severely limit dynamic response, thereby reducing the overall energy harvesting potential [45].

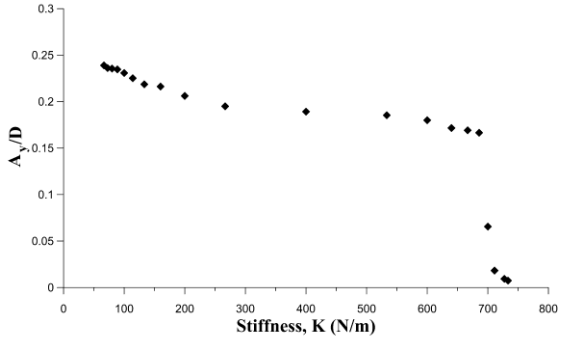

Fig. 6. Amplitude ratio with different stiffness.

The relationship between spring stiffness and the power output of the VIV energy generation system is shown in Fig. 7. The data clearly illustrates the strong sensitivity of power output to both the oscillation amplitude and frequency. At lower stiffness values ranging from 66.7 N/m to 200 N/m, the power output increases steadily from 6.1 W to 5.38 W, representing an overall increase of approximately 51.9%. This trend corresponds to the rise in oscillation frequency accompanied by only a moderate reduction in amplitude. The gradual increase in power output within this stiffness range indicated the system is capable of harvesting energy more efficiently under these conditions, likely due to an optimal balance between structure response and fluid forcing [46].

Power output peaks at 4.90 W when the stiffness is set to 600 N/m, marking the highest value observed across all tested stiffness levels. This peak corresponds to the system's optimal stiffness range, where oscillation frequency reaches approximately 1.986 Hz. At this point, the system achieves and effectively balance between structural compliance and energy transfer, enabling efficient energy extraction from the flow. This result aligns with previous research that emphasize the significance of achieving a resonance condition in VIV systems to maximize energy output [47].

For stiffness values greater than 600 N/m, the power output decreases significantly, falling to 0.0097 W at 733.33 N/m. This substantial decline is primarily due to the drastic reduction in oscillation amplitude from 0.17995 to

0.00745, as the increased stiffness restricts the ability of structure to oscillate and synchronize with vortex shedding frequency [48].

The results demonstrate a clear design trade-off in VIV energy generation systems. While lower stiffness enhances flexibility and increases oscillation amplitude, it compromises structural integrity. Conversely, excessive stiffness suppresses oscillations and significantly reduced power output. These findings emphasize the importance of optimizing stiffness to achieve maximize power generation. The observed peak power at intermediate stiffness values aligns with literature which consistently recommends a balanced stiffness configuration for effective energy harvesting.

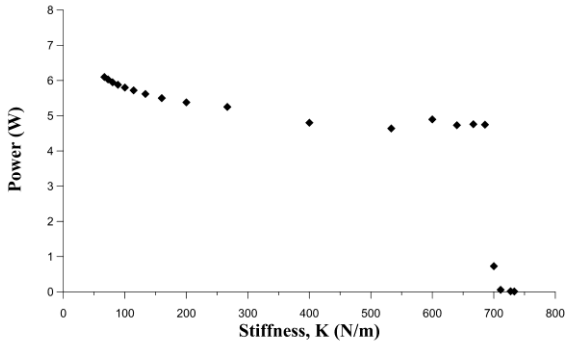

Fig. 7. Maximum power and energy conversion with different stiffness.

The relationship between power-to-volume output and stiffness in VIV energy generation systems is illustrated in Fig. 8. This performance highlights critical insights for optimizing energy harvesting systems to achieve efficient power generation relative to the volume of system. The observed trend together with the associated findings are discussed in the context of existing research on VIV hydrodynamics, reinforcing broader efforts to enhance energy harvesting performance through smart structural parameter tuning.

In the low stiffness ranging from 66.67 N/m to 200 N/m, the power-to-volume output rises steadily, increasing from 1800W/m^3 to 1710 W/m^3. This increase is driven by the combined effects of moderate oscillation amplitudes and a rise in oscillation frequency, which enable the system to harness more energy per unit volume. This trend consistent with observations by Hover et al. (1998) and other studies [49-51], which emphasizing the importance of resonance conditions in enhancing the dynamic response of VIV and maximizing power generation efficiency.

The maximum power-to-volume output is observed at stiffness of 600 N/m, where the system achieves 1529.81 W/m^3. This peak performance corresponds to the ability of system to operate near its resonance frequency, thereby maximizing energy transfer from the fluid to the structure. These findings are consistent with previous study, which have demonstrated that VIV systems optimized for resonance achieve the highest power outputs due to enhanced vortex synchronization and dynamic coupling between structure and the fluid flow [52].

This phenomenon is commonly referred to as "lock-in" and a well-established principle in VIV literature [53].

Beyond this optimal stiffness point, further increases in stiffness shifts the system's natural frequency away from the vortex shedding frequency. As a result, the system falls out of the lock-in range, disrupting the phase synchronization necessary for sustained energy transfer. This loss of synchronization leads to lower vibration amplitudes and reduced oscillatory motion, significantly decreasing the power harvested from the flow [54]. In essence, the structure becomes too rigid to respond effectively to the periodic fluid forces, suppressing the oscillations that are essential for energy generation. Additionally, higher stiffness often corresponds to reduced structural compliance, which limits the deformation capacity required to absorb and convert fluid energy. Studies have consistently shown that energy harvesters tuned away from resonance conditions experience dramatically lower power output due to wakened fluid-structure interactions [55].

For stiffness values exceeding 600 N/m, power-to-volume efficiency decreases sharply. For instance, at a stiffness of 733.33 N/m, the output drop to just 3.04 W/m^3. This decline directly corresponds to the significant reduction in oscillation amplitudes, as excessive stiffness limits the ability of structure to respond dynamically to vortex shedding. Similar effects have been reported in previous study, where excessive stiffness suppressed VIV responses, thereby reducing the efficiency of energy harvesting systems [25].

The results highlight the importance of stiffness tuning for maximizing power-to-volume efficiency. Systems with either excessively low or excessively high stiffness exhibit suboptimal performance, either due to insufficient energy transfer or excessive structural rigidity. The peak efficiency observed at intermediate stiffness values underscores the need to balance compliance and rigidity to achieve ideal performance. This finding consistent with previous study, which have shown that intermediate flexibility produced the most effective VIV response and minimizes energy harvesting capability [29].

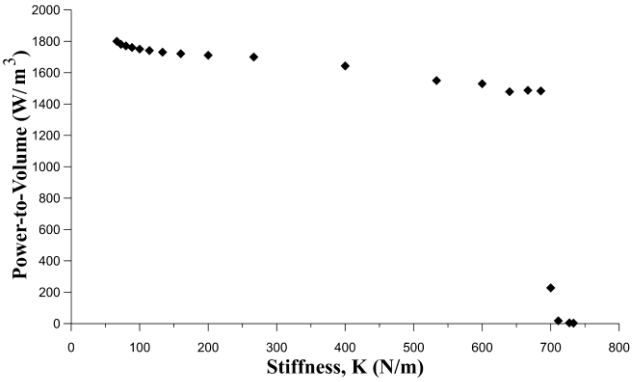

Fig. 8. Maximum power-to-volume density with different stiffness.

Figure 9 presents the vorticity contour fields for two representative stiffness values, approximately 60 N/m and 800 N/m, allowing a detailed comparison of

wake development, vortex formation, and flow–structure interaction across different structural responses. At 60 N/m, the wake pattern shows clearly defined alternating vortices forming a well-organized Kármán vortex street. The vortex structures are coherent and periodically arranged that indicate the strong synchronization between vortex shedding and structural oscillation. This behaviour is typical of the lock-in regime, in which the shedding frequency adjusts to match the natural frequency of the structure. As a result, the flow separation points remain stable, and the vortices grow in size and strength as connected to downstream. The high coherence and regular spacing of the vortices at this stiffness reflect the strong coupling between the fluid forcing and the cylinder motion, which contributes to the relatively high vibration amplitude and enhanced energy transfer observed in this regime.

In contrast, the vorticity contours at approximately 800 N/m reveal a markedly different behaviour. Although vortex shedding remains present, the overall wake becomes broader and exhibits weaker coherence compared to the 60 N/m case. The vortices are less uniform and begin to lose their symmetry, suggesting a partial loss of synchronization between the structural motion and the shedding process. This shift in wake pattern arises because the increased stiffness alters the natural frequency, reducing the degree of frequency matching with the vortex shedding. As a result, the vortices shed from the cylinder show earlier signs of distortion and irregular spacing. Nevertheless, the system still exhibits meaningful flow–structure coupling, which explains why the power extraction remains highest at 60 N/m despite the reduced amplitude. The higher oscillation frequency compensates for the lower displacement, allowing the device to achieve optimal energy conversion efficiency at this stiffness.

When comparing the two stiffness conditions, it is evident that structural stiffness strongly influences wake topology, vortex interaction, and overall VIV behaviour. At low stiffness, the flow separation is more consistent, and the wake width remains narrow due to the stable and synchronized vortex shedding. At higher stiffness, the wake begins to widen, and the vortices display weaker interaction, indicating a transition away from the fully locked-in regime. Similar observations have been reported by previous researchers [56-59], who showed that changes in structural boundary conditions, stiffness, or confinement can alter the vortex strength, shedding period, and wake interaction patterns. In the present study, the vorticity contours clearly demonstrate that the hydrodynamic forces acting on the cylinder are governed by wake stability, synchronization behaviour, and vortex formation modes. As stiffness increases, the flow becomes progressively less organized, leading to reduced amplitude and diminished energy transfer, consistent with the trends observed in amplitude, power, and efficiency.

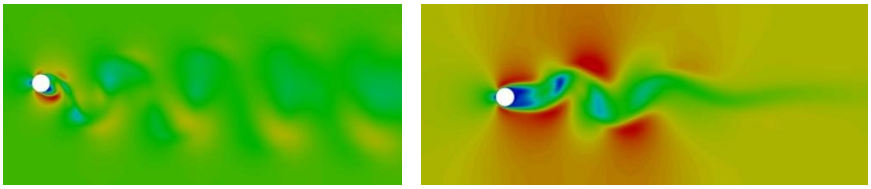

Fig. 9. Vorticity contour of four cylinders, (a) stiffness 60 N/m, (b) stiffness of 800 N/m.

4. Conclusions

In conclusion, the stiffness of the VIV energy generation system plays a critical role in determining its performance. The results reveal relationship between stiffness and key performance outputs, emphasizing the importance of stiffness tuning to achieve optimal system efficiency. Vibration amplitude decreases with increasing stiffness, with a significant peak observed at lower stiffness values due to enhanced structural compliance and resonance effects. Beyond this optimal range, the amplitude diminishes as increased stiffness suppresses oscillatory motion, consistent with established hydrodynamic theories.

The study identifies an optimal stiffness of 60 N/m, where the power output and power-to-volume efficiency are maximized. Beyond this range, excessive stiffness leads to substantial power loss, underscoring the need for precise stiffness tuning in system design. Future research should investigate the effects of additional factors which is damping to further enhance the performance of VIV systems. These advancements will contribute to the development of efficient, compact and sustainable renewable energy solutions suitable for real-world marine environments.

While the present computational study provides valuable insights into the influence of stiffness on VIV energy harvesting performance, several methodological limitations should be acknowledged. The model simplifies some real-world complexities, such as turbulence effects, structural damping variability, and potential multi-mode interactions, which may influence system behaviour. Additionally, only stiffness was systematically varied, while other critical parameters, such as damping and mass ratio were held constant. Future studies should incorporate parametric sensitivity analyses involving damping and fluid properties to provide a more comprehensive performance map. Experimental validation using physical prototypes would further enhance the robustness of the conclusions drawn.

From a practical standpoint, identifying this optimal stiffness range provides essential guidance for the design and tuning of VIV energy generation system in order to achieve maximum energy output while maintaining structural integrity. The findings suggest that choosing the right stiffness value is essential for designing efficient and reliable VIV energy generation system. Proper stiffness tuning can help improve power generation while keeping the device stable and compact, making it more suitable for real marine applications. However, this study has some limitations. The simulation used a single-degree-of-freedom (SDOF) model and assumed a fixed damping ratio and Reynolds number. Real systems may behave differently due to turbulence, structural damping changes, or multi-mode vibrations. These factors could affect the accuracy of the results.

The findings of this study contribute to the fundamental understanding of how structural stiffness tuning influences the performance of VIV energy generation systems. For future work, it is recommended to systematically investigate the effects of variable damping ratios, different mass ratios, and a wider range of flow conditions on VIV performance. Additionally, experimental validation using physical prototypes should be conducted to verify the numerical results and assess real-world feasibility. Further studies should also explore multi-degree-of-freedom models and potential multi-mode interactions to capture more realistic system dynamics. These efforts will support the development of practical, efficient, and sustainable VIV energy generation systems for marine and offshore applications.

Acknowledgement

This research was funded by a grant Fundamental Research Grant Scheme from the Ministry of Higher Education of Malaysia (FRGS Grant Number: FRGS/1/2022/TK06/UMT/02/7, Vot: 59713).

References

1. Gao, Y.; Jiang, Z.; Ma, L.; Fu, S.; He, G.; and Shi, C. (2022). Numerical study of vortex-induced vibrations of a circular cylinder at different incidence angles. *Ocean Engineering*, 259, 111858.
2. Bernitsas, M.M.; Raghavan, K.; Ben-Simon, Y.; and Garcia, E.M.H. (2008). VIVACE (Vortex induced vibration aquatic clean energy): A new concept in generation of clean and renewable energy from fluid flow. *Journal of Offshore Mechanics and Arctic Engineering*, 130(4), 041101.
3. Alias, F.; Zailani, N.S.A.M.; Mohd, M.H.; Kasiman, E.H.; and Rahman, M.A.A. (2024). Numerical simulation on VIV energy harvesting of four cylinders in close staggered formation with different mass ratios. *Journal of Physics*: *Conference Series*, 2688(1), 012007.
4. Alias, F.; and Rahman, M.A.A. (2024). A bibliometric analysis on energy harvesting from vortex-induced vibration. *Cogent Engineering*, 11(1), 2386095.
5. Tang, Z.; and Zhou, B. (2020). The effect of mass ratio and spring stiffness on flow-induced vibration of a square cylinder at different incidence angles. *Ocean Engineering*, 198, 106975.
6. Rahman, M.A.A.; Alias, F.; and Mohd, M.H. (2023). Flow past of a drilling riser system with auxiliary lines in laminar flow. *CFD Letters*, 15(2), 101-113.
7. Alias, F.; Mohd, M.H.; and Rahman, M.A.A. (2021). The influence of incidence angles on flow past a fixed and freely vibrating drilling riser system in laminar flow. *Proceedings of the Thirty-first* (2021) *International Ocean and Polar Engineering Conference* (*ISOPE*), Rhodes, Greece, 2041-2048.
8. Lv, Y.; Sun, L.; Bernitsas, M.M.; and Sun, H. (2021). A comprehensive review of nonlinear oscillators in hydrokinetic energy harnessing using flow-induced vibrations. *Renewable and Sustainable Energy Reviews*, 150, 111388.
9. Modir, A.; and Goudarzi, N. (2019). Experimental investigation of Reynolds number and spring stiffness effects on vortex-induced vibrations of a rigid circular cylinder. *European Journal of Mechanics-B/Fluids*, 74, 34-40.
10. Kang, Z.; Zhang, C.; Chang, R.; and Ma, G. (2019). A numerical investigation of the effects of Reynolds number on vortex-induced vibration of cylinders with different mass ratios and frequency ratios. *International Journal of Naval Architecture and Ocean Engineering*, 11(2), 835-850.
11. Münch, C.; Ausoni, P.; Braun, O.; Farhat, M.; and Avellan, F. (2010). Fluid-structure coupling for an oscillating hydrofoil. *Journal of Fluids and Structures*, 26(6), 1018-1033.
12. Wang, J.; Zhao, W.; Su, Z.; Zhang, G.; Li, P.; and Yurchenko, D. (2020). Enhancing vortex-induced vibrations of a cylinder with rod attachments for hydrokinetic power generation. *Mechanical Systems and Signal Processing*, 145, 106912.

13. Ding, W.; Sun, H.; Xu, W.; and Bernitsas, M.M. (2021). Experimental and computational investigation of interactive flow-induced oscillations of two tandem rough cylinders at $3\times10^4 \leq Re \leq 1.2\times10^5$. *Ocean Engineering*, 223, 108641.
14. Ma, C.; Sun, H.; Nowakowski, G.; Mauer, E.; and Bernitsas, M.M. (2016). Nonlinear piecewise restoring force in hydrokinetic power conversion using flow induced motions of single cylinder. *Ocean Engineering*, 128, 1-12.
15. Stappenbelt, B.; Lalji, F.; and Tan, G. (2007). Low mass ratio vortex-induced motion. *Proceedings of the* 16th *Australasian Fluid Mechanics Conference* (16*AFMC*), Crown Plaza, Gold Coast, Australia, 1491-1497.
16. Zheng, M.; Han, D.; Gao, S.; and Wang, J. (2020). Numerical investigation of bluff body for vortex induced vibration energy harvesting. *Ocean Engineering*, 213, 107624.
17. Wan, H.; and Patnaik, S.S. (2016). Suppression of vortex-induced vibration of a circular cylinder using thermal effects. *Physics of Fluids*, 28(12), 123603.
18. Zahari, M.; Chan, H.B.; Yong, T.H.; and Dol, S.S. (2015). The effects of spring stiffness on vortex-induced vibration for energy generation. *IOP Conference Series*: *Materials Science and Engineering*, 78, 012041.
19. Sanaati, B.; and Kato, N. (2013). Vortex-induced vibration (VIV) dynamics of a tensioned flexible cylinder subjected to uniform cross-flow. *Journal of Marine Science and Technology*, 18(2), 247-261.
20. Martins, F.A.C.; and Avila, J.P.J. (2019). Three-dimensional CFD analysis of damping effects on vortex-induced vibrations of 2DOF elastically-mounted circular cylinders. *Marine Structures*, 65, 12-31.
21. Zhang, J.; Liu, F.; Lian, J.; Yan, X.; and Ren, Q. (2016). Flow induced vibration and energy extraction of an equilateral triangle prism at different system damping ratios. *Energies*, 9(11), 938.
22. Paré-Lambert, O.; and Olivier, M. (2018). A parametric study of energy extraction from vortex-induced vibrations. *Transactions of the Canadian Society for Mechanical Engineering*, 42(4), 359-369.
23. Arionfard, H.; and Nishi, Y. (2017). Experimental investigation of a drag assisted vortex-induced vibration energy converter. *Journal of Fluids and Structures*, 68, 48-57.
24. Barrero-Gil, A.; Pindado, S.; and Avila, S. (2012). Extracting energy from vortex-induced vibrations: A parametric study. *Applied Mathematical Modelling*, 36(7), 3153-3160.
25. Sun, H.; Kim, E.S.; Nowakowski, G.; Mauer, E.; and Bernitsas, M.M. (2016). Effect of mass-ratio, damping, and stiffness on optimal hydrokinetic energy conversion of a single, rough cylinder in flow induced motions. *Renewable Energy*, 99, 936-959.
26. Dahl, J.M.; Hover, F.S.; and Triantafyllou, M.S. (2006). Two-degree-of-freedom vortex-induced vibrations using a force assisted apparatus. *Journal of Fluids and Structures*, 22(6-7), 807-818.
27. Ding, C.; Srinil, N.; Bao, Y.; Zhou, D.; and Han, Z. (2020). Vortex-induced vibrations of two mechanically coupled circular cylinders with asymmetrical stiffness in side-by-side arrangements. *Journal of Fluids and Structures*, 95, 102995.

28. Gonçalves, R.T.; Sakata, K.; Gambarine, D.M.; Cicolin, M.M.; Hirabayashi, S.; and Assi, G.R.S. (2018). Experimental study on vortex-induced vibration of floating circular cylinders with low aspect ratio and different free-end corner shapes. *Proceedings of the ASME* 2018 37th *International Conference on Ocean, Offshore and Arctic Engineering*, Madrid, Spain, V002T08A035.
29. Gonçalves, R.T.; Meneghini, J.R.; and Fujarra, A.L.C. (2018). Vortex-induced vibration of floating circular cylinders with very low aspect ratio. *Ocean Engineering*, 154, 234-251.
30. Zhao, M.; Kaja, K.; Xiang, Y.; and Cheng, L. (2016). Vortex-induced vibration of four cylinders in an in-line square configuration. *Physics of Fluids*, 28(2), 023602.
31. Zhao, M.; and Cheng, L. (2014). Vortex-induced vibration of a circular cylinder of finite length. *Physics of Fluids*, 26(1), 15111.
32. Gao, Z.; Li, Z.; Niu, J.; Yin, Q.; and Liu, K. (2023). Application of nonlinear stiffness mechanism on energy harvesting from vortex-induced vibrations. *Frontiers in Marine Science*, 10, 1270286.
33. Gambarine, D.M.; Minioli, L.E.B.; Gonçalves, R.T.; Kogishi, A.M.; and Fujarra, A.L.C. (2018). Influence of stiffness ratio on vortex-induced vibration of cylinder with low aspect ratio. *Proceedings of the ASME* 2018 37th *International Conference on Ocean, Offshore and Arctic Engineering*, Madrid, Spain, V002T08A055.
34. Wu, X.; Ge, F.; and Hong, Y. (2012). A review of recent studies on vortex-induced vibrations of long slender cylinders. *Journal of Fluids and Structures*, 28, 292-308.
35. Chen, L.; Dong, Y.; and Wang, Y. (2021). Flow-induced vibration of a near-wall circular cylinder with a small gap ratio at low Reynolds numbers. *Journal of Fluids and Structures*, 103, 103247.
36. Rahman, M.A.A.; Leggoe, J.; Thiagarajan, K.; Mohd, M.H.; and Paik, J.K. (2015). Numerical simulations of vortex-induced vibrations on vertical cylindrical structure with different aspect ratios. *Ships and Offshore Structures*, 11(4), 405-423.
37. Wang, Y.; Cheng, W.; Du, R.; Wang, S.; and Deng, Y. (2020). Numerical investigation of flow around two tandem identical trapezoidal cylinders. *Mathematical Problems in Engineering*, 2020, 3759834.
38. Alias, F.; Mohd, M.H.; and Rahman, M.A.A. (2024). The influence of different mass ratios on vortex-induced vibration energy extraction of four-cylinder arrays. *Journal of Advanced Research in Fluid Mechanics and Thermal Sciences*, 117(2), 1-14.
39. Han, P.; Huang, Q.; Pan, G.; Qin, D.; Wang, W.; Rodolfo T. Gonçalves, R.T.; and Zhao, J. (2023). Optimal energy harvesting efficiency from vortex-induced vibration of a circular cylinder. *Ocean Engineering*, 282, 114869.
40. Alias, F.; Mohd, M.H.; Musa, M.A.; Kasiman, E.H.; and Rahman, M.A.A. (2021). Flow past a fixed and freely vibrating drilling riser system with auxiliaries in laminar flow. *Journal of Advanced Research in Fluid Mechanics and Thermal Sciences*, 87(3), 94-104.
41. Zhang, B.; Mao, Z.; Song, B.; Tian, W.; and Ding, W. (2018). Numerical investigation on VIV energy harvesting of four cylinders in close staggered formation. *Ocean Engineering*, 165, 55-68.

42. Canilho, H.; Fael, C.; and Páscoa, J. (2020). A numerical study of the effect of vortex-induced vibrations on a circular cylinder mounted under elastic support. *KnE Engineering*, 2020, 100-112.
43. Song, Z.; Duan, M.; and Gu, J. (2017). Numerical investigation on the suppression of VIV for a circular cylinder by three small control rods. *Applied Ocean Research*, 64, 169-183.
44. Irawan, Y.H.; Raza, S.A.; and Chern, M.J. (2022). Numerical predictions of vibration responses and flow energy conversion efficiency of side-by-side cylinders at moderate Reynolds number. *Applied Ocean Research*, 129, 103392.
45. Park, H.; Kumar, R.A.; and Bernitsas, M.M. (2016). Suppression of vortex-induced vibrations of rigid circular cylinder on springs by localized surface roughness at $3\times10^4 \leqslant \mathrm{Re} \leqslant 1.2\times10^5$. *Ocean Engineering*, 111, 218-233.
46. Yuan, W.; Sun, H.; Li, H.; and Bernitsas, M.M. (2020). Flow-induced oscillation patterns for two tandem cylinders with turbulence stimulation and variable stiffness and damping. *Ocean Engineering*, 218, 108237.
47. Sun, H.; Ma, C.; Kim, E.S.; Nowakowski, G.; Mauer, E.; and Bernitsas, M.M. (2017). Hydrokinetic energy conversion by two rough tandem-cylinders in flow induced motions: Effect of spacing and stiffness. *Renewable Energy*, 107, 61-80.
48. Bearman, P.W. (2011). Circular cylinder wakes and vortex-induced vibrations. *Journal of Fluids and Structures*, 27(5-6), 648-658.
49. Reyes, M.; and Mandujano, F. (2022). Vortex induced vibrations of a cylinder at low mass ratio. *European Journal of Mechanics-B/Fluids*, 91, 66-79.
50. Ding, L.; Zhang, L.; Bernitsas, M.M.; and Chang, C.-C. (2016). Numerical simulation and experimental validation for energy harvesting of single-cylinder VIVACE converter with passive turbulence control. *Renewable Energy*, 85, 1246-1259.
51. Yang, X.; Saevik, S.; and Sun, L. (2015). Numerical analysis of buckling failure in flexible pipe tensile armor wires. *Ocean Engineering*, 108, 594-605.
52. Sun, H.; Li, H.; Yang, N.; Hou, G.; and Bernitsas, M.M. (2023). Experimental and numerical study of the shielding effect of two tandem rough cylinders in flow-induce oscillation. *Marine Structures*, 89, 103374.
53. Xing, J.; Rezaei, M.; Dai, H.; and Liao, W.-H. (2024). Investigating the coupled effect of different aspect ratios and leeward protrusion lengths on vortex-induced vibration (VIV)-galloping energy harvesting: Modelling and experimental validation. *Journal of Sound and Vibration*, 568, 118054.
54. Li, Z.; Zhang, H.; Litak, G.; and Zhou, S. (2024). Periodic solutions and frequency lock-in of vortex-induced vibration energy harvesters with nonlinear stiffness. *Journal of Sound and Vibration*, 568, 117952.
55. Fang, S.; Du, H.; Yan, T.; Chen, K.; Li, Z.; and Zhou, S. (2024). Theoretical and experimental investigation on the advantages of auxetic nonlinear vortex-induced vibration energy harvesting. *Applied Energy*, 356, 122395.
56. Silva-Ortega, M.; and Assi, G.R.S. (2018). Hydrodynamic loads on a circular cylinder surrounded by two, four, and eight wake-control cylinders. *Ocean Engineering*, 153, 345-352.

57. Chen, W.; Ji, C.; Williams, J.; Xu, D.; Yang, L.; and Cui, Y. (2018). Vortex-induced vibrations of three tandem cylinders in laminar cross-flow: Vibration response and galloping mechanism. *Journal of Fluids and Structures*, 78, 215-238.
58. Assi, G.R.S.; Meneghini, J.R.; Aranha, J.A.P.; Bearman, P.W.; and Casaprima, E. (2006). Experimental investigation of flow-induced vibration interference between two circular cylinders. *Journal of Fluids and Structures*, 22(6-7), 819-827.
59. Lou, M.; Chen, P.; and Chen, Z. (2017). Experimental investigation on the suppression of vortex-induced vibration of two interfering risers by control rods. *Ships and Offshore Structures*, 12(8), 1117-1126.